Original scientific paper
https://doi.org/10.33180/InfMIDEM2024.206

Informacije MIDEM
Journal of Microelectronics,
Electronic Components and Materials
Vol. 54, No. 2(2024), 131 – 147

A Novel Dual-Mode Dual Type Hysteresis Schmitt Trigger and its Applications using Single Differential Voltage Current Conveyor Transconductance Amplifier

Harika Pamu, Puli Kishore Kumar, Kiran Kumar Gurrala

Department of Electronics and Communication Engineering, National Institute of Technology Andhra Pradesh, Tadepalligudem, Andhra Pradesh, India

Abstract: This paper introduces a novel Schmitt trigger circuit that can operate in two modes: voltage and trans-impedance mode using a sole Differential Voltage Current Conveyor Transconductance Amplifier (DVCCTA) within the same topology with external grounded resistors. The suggested designs enable dual-type hysteresis (clockwise (CW) and counter-clockwise (CCW)) simultaneously within the same circuit topology. Additionally, the proposed design includes the unique ability to control threshold levels through the transconductance parameter (g_m) of DVCCTA via a grounded resistor. The proposed Schmitt trigger is extended for the application of a square/triangular waveform generator and pulse width modulator to illustrate the utility of the given Schmitt trigger circuit. All the proposed designs are appropriate for IC integration due to the available grounded passive attributes. Moreover, the design comes with a feature of independent control of oscillation frequency using a grounded capacitor eliminates the highest level of parasitics, and lessens the circuit's sensitivity to noise immunity. The maximum absolute deviation of output amplitude is observed to be less than 0.062 % (for CW mode) and 0.038 % (for CCW mode), while for threshold voltages, it is below 0.528 % (CW) and 0.321 % (CCW), respectively against for temperature variations of 0- 100 °C. Realization of DVCCTA uses 20 MOS transistors with 0.18 µm TSMC CMOS technology parameter, which is used to authenticate the workableness of the proposed design through PSPICE. Additionally, Monte Carlo simulations, temperature-dependent variations, non-ideal analysis, schematic layout with post-layout simulation, and also experimental results using ICAD844 are presented to validate the proposed design. The simulated responses correlate with the theoretical prediction.

Keywords: Schmitt trigger, DVCCTA, dual-type hysteresis, Square/triangular waveform generator, electronically tunable, pulse width modulation (PWM)

Nov dvonivojski histerezni Schmittov prožilec in njegova uporaba z uporabo enojnega diferencialnega napetostnega tokovnega transkonduktančnega ojačevalnika

Izvleček: Članek predstavlja novo vezje Schmittovega prožilca, ki lahko deluje v dveh načinih: v napetostnem in transimpedančnem načinu z uporabo enega diferencialnega napetostno tokovnega transkonduktančnega ojačevalnika (DVCCTA) znotraj iste topologije z zunanjimi ozemljenimi upori. Predlagane zasnove omogočajo dvojno histerezo (v smeri urinega kazalca (CW) in v nasprotni smeri urinega kazalca (CCW)) znotraj iste topologije vezja. Poleg tega predlagana zasnova vključuje edinstveno zmožnost nadzora pragovnih ravni preko parametra transkonduktance (g_m) DVCCTA z ozemljenim uporom. Predlagani Schmittov prožilec je razširjen za uporabo generatorja pravokotnih/trikotnih valovnih oblik in modulatorja širine impulzov, da se ponazori uporabnost danega vezja Schmittovega prožilca. Vse predlagane zasnove so zaradi razpoložljivih ozemljenih pasivnih gradnikov primerne za integracijo v IC. Poleg tega je zasnova opremljena s funkcijo neodvisnega nadzora frekvence nihanja z uporabo ozemljenega kondenzatorja, ki odpravlja raven parazitnih signalov in zmanjšuje občutljivost vezja na šum. Največje absolutno odstopanje izhodne amplitude je

How to cite:
H. Pamu et al., "A Novel Dual-Mode Dual Type Hysteresis Schmitt Trigger and its Applications using Single Differential Voltage Current Conveyor Transconductance Amplifier", Inf. Midem-J. Microelectron. Electron. Compon. Mater., Vol. 54, No. 2(2024), pp. 131–147

manjše od 0,062 % (v načinu CW) in 0,038 % (v načinu CCW), medtem ko je za mejne napetosti pod 0,528 % (CW) oziroma 0,321 % (CCW) pri temperaturnih spremembah od 0 do 100 °C. Realizacija DVCCTA uporablja 20 tranzistorjev MOS s tehnologijo CMOS TSMC 0,18 µm, ki se uporablja za preverjanje uporabnosti predlagane zasnove s PSPICE. Poleg tega so za potrditev predlagane zasnove predstavljene simulacije Monte Carlo, temperaturno odvisne variacije, neidealna analiza, shematska postavitev s simulacijo po postavitvi in tudi eksperimentalni rezultati z uporabo ICAD844. Simulirani odzivi se ujemajo s teoretičnimi napovedmi.

Ključne besede: Schmittov prožilec, DVCCTA, dvojna histereza, generator pravokotnih/trikotnih valov, elektronska nastavljivost, pulzno-širinska modulacija (PWM)

** Corresponding Author's e-mail: harikapamu.sclr@nitandhra.ac.in*

1 Introduction

The present world of the electronics environment is augmented with filters, rectifiers, amplifiers, A/D converters, comparators, oscillators, and many more signal-processing circuits. Among these, a comparator circuit accompanied by positive feedback is named as Schmitt trigger [1] which plays a vital role in the province of both analog and digital. Schmitt trigger circuit transforms any irregularly formed input signal into a square waveform and is commonly used to improve the circuit's immunity to noise. In addition, it is an essential block used in distinct applications like a square waveform generator [2], versatile modulator [3], relaxation oscillators [4], function generators [5], monostable multivibrator [6], pulse width modulator [7], switching power supplies [8], etc.

Initially, a Schmitt trigger has been presented with a traditional Op-Amp and passive components [1] but suffers from a finite gain-bandwidth product, high power dissipation, low slew rate, lesser dynamic range, etc. [9]. As an attractive strategy to waver the constraints of conventional Op-Amp [10], Various current mode analog active blocks (AAB) have been reported in the literature namely (second generation current conveyor) CCII [11], (third generation current conveyor) CCIII [12], (operational transconductance amplifier) OTA [13], (operational trans resistance amplifier) OTRA [14], (differential voltage current conveyor) DVCC [15], (dual X current conveyors) DXCCII [16], (dual X current conveyor transconductance amplifier) DXCCTA [17] and many more. An active block namely DVCCTA is chosen from the above-cited current mode active blocks due to its prominent feature of electronically adjustable transconductance in comparison to Op-Amp. The usage of DVCCTA can be extended to the field of signal processing for designing various circuits namely analog filters [18] - [19], oscillators[20] - [21], simulator [22] and so many.

Numerous Schmitt trigger circuit implementations using distinct current mode AAB are reported in the literature [23-43]. Some circuits based on CCII are discussed in [23]–[27], but these implementations require either a higher number of active or passive elements and are incapable of providing a dual-type hysteresis mode of operation. In [27], a non-inverting Schmitt trigger is demonstrated, employing only a CCII and three passive components. This circuit functions as a zero-voltage comparator and is capable of adjusting the threshold voltage levels. However, a Schmitt trigger with independent current control of amplitude and frequency using two OTA's along with two grounded resistors is cited in [28]. In [29], current input dual hysteresis mode OTRA Schmitt trigger has been delivered with the possibility of changing its type of hysteresis with the help of a switch. Although, it uses a floating resistor which is not an advisable feature for IC Implementation. The improvement in circuit design using DXCCTA is also given in [30] without any passive elements. This configuration reduces the influence of temperature variation on output amplitude levels. However, it doesn't offer the capability to demonstrate both CW and CCW hysteresis. Another prominent configuration with DVCC and two grounded resistors [31] has the capability to adjust the hysteresis by varying the values of a resistor. Two more designs with (differential difference current conveyor) DDCC and (current differencing transconductance amplifier) CDTA with two resistors are demonstrated in [32] and [33] but unable to exhibit dual type hysteresis. Aside from the above mentioned circuits, dual-type hysteresis, independent and electronic control of threshold and amplitude levels are viable through (current follower differential input transconductance amplifier) CFDITA [34], (current differencing buffered amplifier) CDBA [35], (current controlled current differencing transconductance amplifier) CCCDTA [36] based designs but circuit in [34] is unable to give both type of hysteresis simultaneously. The Schmitt trigger circuit mentioned in [37] that uses a single (voltage differencing transconductance amplifier) VDTA and one resistor is unable to exhibit dual type hysteresis, but it does have the ability to independently control the output amplitude levels. Circuit cited in [38] uses single (second generation current controlled current conveyor) CCCII, a capacitor and two resistors for generating

a square waveform with the maximum power consumption of 600 µW but unable to exhibit dual-type hysteresis. Square wave generators based on (second generation differential current conveyor) DCII, two resistors and a sole capacitor in [39] and [40] have the advantage of reducing noise caused by parasitics through the use of a grounded capacitor. A recent proposal introduces a Waveform generator utilizing commercially available ICs along with (extra X second generation current conveyor) EXCCII prototype [42] and five passive components. The circuit benefits from the capability of independently controlling oscillation frequency via passive elements. Also, an attempt was made to design a Schmitt trigger with (second generation voltage conveyor) VCII [43] comprising of two active blocks and five resistors exhibiting an average power consumption of 328 µW and 365 µW for transitions at non-inverting and inverting mode outputs, respectively. Table. 1 demonstrates a comparative study with the earlier described Schmitt trigger circuits, which is summarized in the comparison section in great detail.

Henceforth, this paper presents a Schmitt trigger with dual-type hysteresis within the same topology available in two modes specifically voltage and trans-impedance mode with less number of grounded passive components and its application as a square/triangular wave generator and pulse width modulator. The design works with an AAB named DVCCTA for the Schmitt trigger operation. Additionally, the proposed design comes with an attractive feature of availability of both modes (voltage and transimpedance) within the same circuit topology. Notably, the topologies provide the benefit of independent control of threshold levels and oscillation frequency. The simulation results using PSPICE along with CMOS based DVCCTA and the ex-

Table. 1: Comparison of the proposed Schmitt trigger topology with the existing literature

Ref	Type and no. of AAB used	No. of passive component used	All grounded passive elements	Dual Type Hysteresis	Transistor type or IC	Dual type Hysteresis within the same topology	Operational frequency (HZ)	Independent control of threshold levels	Independent control of oscillation frequency	Insensitive to Temperature	Experimental Results Shown
[23]	CCII – 2	4 R	No	No	0.6 µm CMOS, IC AD844	No	10K	No	No	No	Yes
[24]	CCII – 1	3R	No	No	0.35 µm AMS CMOS	No	-	No	No	NA	No
[25]	CCII – 2	6R, 1C	No	No	0.35 µm AMS CMOS	No	-	No	Yes	No	No
[27]	CCII – 1	3R	No	No	0.35 µm AMS CMOS	No	-	No	Yes	NA	Yes
[28]	OTA – 2	2R	Yes	No	LM13600N	No	-	Yes	Yes	No	No
[29]	OTRA – 1	1R	No	Yes	IC AD844	Yes	100K	No	No	NA	No
[30]	DXCCTA–1	No	NA	No	TSMC 180 nm CMOS	No	5M	Yes	No	Yes	No
[31]	DVCC – 1	2R	Yes	No	0.25 µm CMOS, OPA660	No	400K	Yes	Yes	NA	Yes
[32]	DDCC- 1	2R	No	No	0.5 µm MIETTEC	No	NA	No	No	No	No
[33]	CDTA- 1	2R	No	No	0.18 µm CMOS	No	410K	No	Yes	No	Yes
[34]	CFDITA – 1	1R	Yes	Yes	IC AD844, LM13700	Yes	5K	Yes	No	NA	Yes
[35]	CDBA- 1	3R	No	Yes	IC AD844	No	50	No	No	Yes	Yes
[36]	CCCDTA – 1	No	NA	Yes	IC AD844, ALA400 BJT and LM13600 N	Yes	100K	Yes	Yes	No	Yes
[37]	VDTA – 1	1R	Yes	No	BJT ALA400	No	1K	Yes	No	NA	No
[38]	CCCII – 1	2R,1C	Yes	No	45 nm BSIM CMOS, ICAD844	No	4M	No	No	No	Yes
[39]	DCII – 1	2R,1C	No	No	gpdk 180 nm	No	3.8M	No	Yes	No	Yes
[40]	DCII – 1	2R,1C	No	No	gpdk 180 nm	No	NA	No	Yes	No	Yes
[41]	VDTA-R – 1	2R	Yes	Yes	0.25 µm TSMC	Yes	NA	Yes	Yes	No	No
[42]	EXCCII – 1	3R	No	No	IC AD844	No	19.2K	No	Yes	No	Yes
[43]	VCII – 2	5R	No	Yes	0.18 µm CMOS	Yes	NA	Yes	No	NA	No
Proposed Design	DVCCTA – 1	1R	Yes	Yes	0.18 um TSMC and IC AD844	Yes	5M	Yes	Yes	Yes	Yes

perimental verification using IC AD844 are examined to authenticate the theory. Also, the feasibility of Schmitt trigger for different type of input voltages, temperature dependence, non-ideal analysis, and Monte Carlo analysis is illustrated.

The remaining sections of the paper are structured as follows. Section 2 discusses the circuit representation and analysis of the basic building block DVCCTA and the proposed dual mode (voltage mode and transimpedance mode) Schmitt trigger. Section 3 focuses on how the proposed circuits can be extended for the application as a square/triangular waveform generator and pulse width modulator. Section 4 gives the effect of non-ideal current and voltage transfer gains on the performance of the proposed Schmitt trigger. Section 5 presents the functional verification of the proposed circuits through simulation results. Moving on to Section 6 gives further validation of the proposed designs through experimental analysis, followed by a comparative analysis with existing models in Section 7. Finally, Section 8 addresses the conclusion.

2 Circuit representation and analysis

2.1 DVCCTA

The DVCCTA, a simple active block was first given in [44], which is combination of DVCC [15] resides at input phase and OTA [13] remains at output phase, which is a combination of DVCC [15] resides at input phase and OTA [13] remains at the output phase. Fig. 1 depicts the hierarchical block, while Fig. 2 presents the commercially available IC AD844 implementation and CMOS implementation [49] of DVCCTA, respectively.

The following characteristic equations define the analog block as:

$$I_{Y1} = I_{Y2} = 0; V_X = V_{Y1} - V_{Y2};\ I_{Z+} = I_X; I_{O-} = -g_m V_{Z+} \quad (1)$$

where g_m can be defined as the transconductance of DVCCTA. This parameter is electronically tunable via an external biasing current (I_B) which is described by the following equation (2).

$$g_m = \sqrt{\mu_n c_{ox} \left(\frac{W}{L}\right)_{11,12} I_B} \quad (2)$$

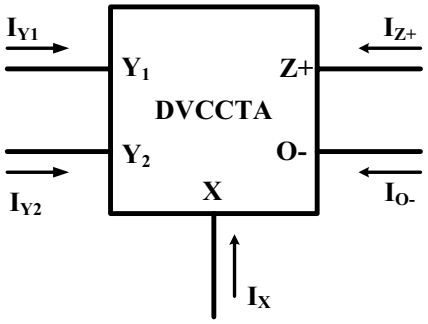

Figure 1: Hierarchical block of DVCCTA

(a)

(b)

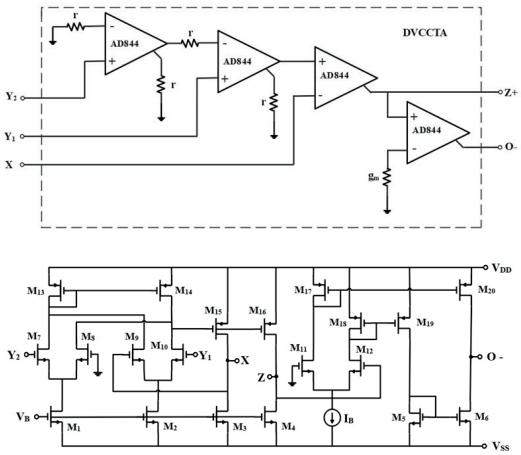

Figure 2: DVCCTA **(a)** IC AD844 implementation **(b)** CMOS implementation

2.2 DVCCTA based voltage mode Schmitt trigger

The proposed voltage mode Schmitt trigger uses a single DVCCTA and only one grounded external resistor with inputs V_{in1}, $V_{in2,}$ and output V_{out} is shown in Fig. 3. With the selection of input, we can avail dual type hysteresis operation likely CW and CCW which are clearly disclosed below.

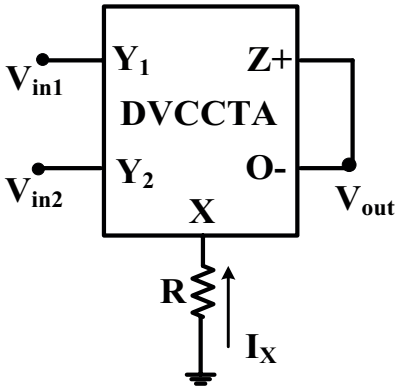

Figure 3: Proposed voltage mode Schmitt trigger circuit

2.2.1. CCW Schmitt trigger

Here, to enable the CCW mode of operation, the input V_{in1} is driven through the Y_1 terminal of DVCCTA by keeping Y_2 terminal grounded. The output V_{out} is taken across the O- terminal of DVCCTA. Depending upon the input signal level, square wave output either saturates at (positive saturation level) + V_{sat} or at the (negative saturation level) - V_{sat}.

From the routine analysis of the design,

$$I_X = \frac{V_X}{R} \tag{3}$$

Adopting the port relation of DVCCTA ($V_X = V_{Y1} - V_{Y2}$), and $V_{Y2} = 0$; $V_X = V_{Y1} = V_{in1}$. Equation (2) can be written as

$$I_X = \frac{V_{in1}}{R} \tag{4}$$

Here the currents passing through the terminals Z+ and O- are equal ($I_{Z+} = I_{O-}$) because of the short circuit connection. From the port relations ($I_{Z+} = I_X$; $I_{O-} = -g_m V_{Z+}$) given in equation (1), we can write as follows

$$I_X = -g_m V_{Z+} \tag{5}$$

Using equations (4 and 5) and from circuit $V_{Z+} = V_{out}$, the input voltage (V_{in1}) is expressed as:

$$V_{in1} = \left(-g_m V_{Z+}\right) R = -V_{out}\left(\frac{R}{R_m}\right) \tag{6}$$

where g_m is taken as $1/R_m$.

The upper threshold voltage (V_{TH}) is calculated with the assumption that the initial value of output is at -V_{sat}.

$$V_{TH} = +V_{sat}\left(\frac{R}{R_m}\right) \tag{7}$$

As V_{in1} increases from zero, V_{out} remains at -V_{sat} until V_{in1} reaches V_{TH}. When it satisfies the condition ($V_{in1} > V_{TH}$), output level changes from -V_{sat} to +V_{sat}. Subsequently, the low threshold voltage (V_{TL}) is given as

$$V_{TL} = -V_{sat}\left(\frac{R}{R_m}\right) \tag{8}$$

The output level (+V_{sat}) is maintained for the input $V_{in1} > V_{TL}$.

The corresponding value for the hysteresis is calculated as

$$V_{HYS} = V_{TH} - V_{TL} \tag{9}$$

2.2.2 CW Schmit trigger

This mode of operation is supervised by V_{in2} through the inverting Y_2 terminal of DVCCTA since V_{in1} is grounded. The O terminal comprises for output V_{out}, as shown in Fig. 3. The circuit analysis is as same as CCW mode and the voltage V_{in2} can be expressed as

$$V_{in2} = V_{out}\left(\frac{R}{R_m}\right) \tag{10}$$

The hysteresis operation is observed to be adverse of CCW operation with the assumption that the initial value of output is at +V_{sat}. Therefore, V_{TH} and V_{TL} are observed to be same as in equations (7) and (8) respectively.

2.3 Transimpedance mode Schmitt trigger

The transimpedance mode Schmitt trigger circuit is realized using the same topology as in Fig. 3 by adding an external grounded resistors at Y terminals with a current input (I_{in}). Dual-type hysteresis is available within same topology with the selection of input as either I_{in1} or I_{in2} within the same design and is clearly disclosed in this section.

CCW transimpedance mode Schmitt trigger is enabled through the input I_{in1} at Y_1 terminal of DVCCTA when Y_2 terminal is grounded and the output V_{out} is observed at O terminal of DVCCTA which is shown in Fig. 4. The principle operation is same as the voltage mode Schmitt trigger by considering the initial value of output is at -V_{sat}. By considering the ideal characteristics from equation (1), the simple calculations can be obtained below:

The input current (I_{in1}) is expressed as

$$I_{in1} = -V_{out}\left(\frac{R}{R_1}\right) g_m \tag{11}$$

Where g_m is taken as $1/R_m$.

The upper and lower threshold currents (I_{TH}, I_{TL}) can be expressed to be

$$I_{TH} = +V_{sat}\left(\frac{R}{R_1 R_m}\right) \tag{12}$$

$$I_{TL} = -V_{sat}\left(\frac{R}{R_1 R_m}\right) \tag{13}$$

CW transimpedance mode Schmitt trigger is enabled through the input I_{in2} at Y_2 terminal of DVCCTA while the other input terminal Y_1 is grounded. The O terminal incorporates the output V_{out} where the operation of hysteresis is observed to be adverse of CCW type. Likewise, the input current (I_{in2}) is given in equation (14) and I_{TH}, I_{TL} are the same as of CW type since the initial assumption of output is settled at $+V_{sat}$.

$$I_{in2} = V_{out}\left(\frac{R}{R_2}\right)g_m \tag{14}$$

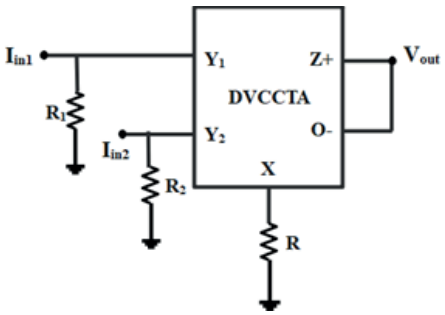

Figure 4: Transimpedance mode Schmitt trigger circuit

3 Applications

3.1 Waveform generator

To illustrate the usefulness and practical application of the introduced work, Schmitt trigger-based square/triangular waveform generator is depicted in Fig. 5. The waveform generator incorporates the proposed voltage mode Schmitt trigger design along with an integrator using CFOA, a resistor, and a capacitor. The proposed scheme adopts only grounded passive components. Mostly, the grounded capacitor reduces the level of parasitics during fabrication. It is expanded to the waveform generator as a square wave at V_{out1} and triangular wave at V_{out2} output terminals, that can be mathematically characterized as:

$$V_{out1} = V_{square} = -\frac{R_m}{R}V_{in} \tag{15}$$

$$V_{out2} = V_{triangular} = -\frac{V_{square}}{R_0 S C_0} \tag{16}$$

The Schmitt trigger either saturates at $+V_{sat}$ or $-V_{sat}$. Initially, by assuming that the output V_{square} is at $+V_{sat}$, this voltage makes the capacitor C_0 to charge with current I_Z initiating V_{out2} to linearly increase with a positive slope until V_{TH}. Subsequently, the square waveform output changes to $-V_{sat}$ which makes the capacitor C_0 to discharge V_{out2} decreases linearly with a negative slope until it reaches V_{TL} of V_{out1}. The succeeding relationships provide charging and discharging intervals of the capacitor.

$$\frac{V_{TH} - V_{TL}}{T_1} = \frac{I_Z}{C_0} \tag{17}$$

$$\frac{V_{TL} - V_{TH}}{T_2 - T_1} = -\frac{I_Z}{C_0} \tag{18}$$

Whereas V_{TH} and V_{TL} are originated from Equations (7) and (8), the time period ($T = T_1 + T_2$) of the waveform and subsequently the frequency can be computed as

$$T = 6RC_0 \tag{19}$$

$$f = \frac{1}{6RC_0} \tag{20}$$

3.2 Pulse Width Modulator (PWM)

PWM scheme is extensively used in voltage regulation, communication systems, power conversion control circuits, ADC, Instrumentation systems, and digital audio [45]–[48]. In this technique, the pulse width of the modulated output is altered according to the voltage level of input modulating signal. PWM output signal can be more oftenly produced by comparing a modulating signal and a carrier waveform like triangular or sawtooth waveform. The proposed design is adequately suited for designing the Pulse Width Modulator (PWM) displayed in Fig. 6 consists of single DVCCTA which acts as a comparator and a resistor. The modulating signal V_{in} is given through input terminal Y_2, the voltage across Y_1 terminal Y_C operate as a carrier signal and the required PWM output V_{out} is taken over the Z terminal of DVCCTA. The feasible saturation levels of V_{out} are $+V_{sat}$ and $-V_{sat}$. As the V_C increases from zero and moves towards the input modulating signal V_{in}, the PWM output voltage abides at $-V_{sat}$ and once V_C reaches V_{in} and satisfies the condition ($V_C > V_{in}$), V_{out} changes its state from $-V_{sat}$ to $+V_{sat}$. It is maintained until the carrier voltage decreases and satisfies the condition of ($V_C < V_{in}$), then the PWM output state changes to $-V_{sat}$.

Employing the terminal characteristics given in equation (1), the mathematical analysis is given below

$$V_X = V_C - V_{in} \tag{21}$$

The current through X terminal can be written as

$$I_X = \frac{V_C - V_{in}}{R} \tag{22}$$

As we know that, from equation (1), $I_{Z+} = I_X$ and $I_{O-} = -g_m V_Z$. Therefore, by equating I_{Z+} and I_{O-} because of the short circuit connection.

$$I_X = -g_m V_{out} = \frac{-V_{out}}{R_m} \tag{23}$$

Where g_m is considered as $1/R_m$.

By making use of equations (22, 23), the output voltage V_{out} of PWM is determined as

$$V_{out} = \frac{R_m}{R}\left(V_{in} - V_C\right) \tag{24}$$

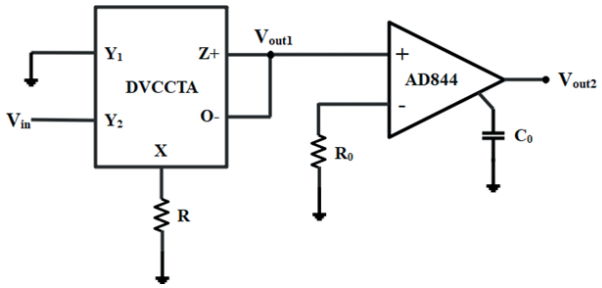

Figure 5: Square/triangular wave generator

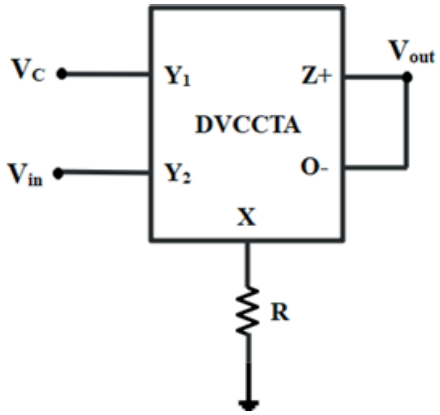

Figure 6: Proposed Pulse Width Modulator (PWM)

4 Non ideal analysis

To determine the non-ideal response of the proposed Schmitt Trigger, including various non-idealities of DVCCTA. The tracking errors in the matrix below show the deviation from the ideal DVCCTA's properties.

$$\begin{bmatrix} I_{Y1} \\ I_{Y2} \\ V_X \\ I_Z \\ I_{O\pm} \end{bmatrix} = \begin{bmatrix} 0 & 0 & 0 & 0 \\ 0 & 0 & 0 & 0 \\ 0 & \beta_1 & -\beta_2 & 0 \\ \alpha & 0 & 0 & 0 \\ 0 & 0 & 0 & \pm\gamma g_m \end{bmatrix} \begin{bmatrix} I_X \\ V_{Y1} \\ V_{Y2} \\ V_Z \end{bmatrix} \tag{25}$$

Here, α represents the current transfer gain, while β_1 and β_2 denote the voltage transfer gains, and γ represents the transconductance gain. The numerical relation between α and the current tracking error (ξ_i), as well as β and the voltage tracking error (ξ_v), can be expressed as:

$$\alpha = 1 - \xi_i,\ \beta_1 = 1 - \xi_{v_1} \text{ and } \beta_1 = 1 - \xi_{v_2} \tag{26}$$

Further analysis of the proposed circuits using equation (25) is as follows:

For CCW operation, By taking, $V_X = \beta_1 V_{in1}$ and $V_{Y2} = 0$, equation (3) can be written as

$$I_X = \frac{\beta_1 V_{in1}}{R} \tag{27}$$

Also considering, ($I_{Z+} = \alpha I_X$; $I_{O-} = -\gamma g_m V_{Z+}$), equation (5) can be written as

$$\alpha I_X = -\gamma g_m V_{Z+} \tag{28}$$

From equations (27 & 28), the input voltage V_{in1} is expressed as

$$V_{in1} = \frac{\gamma}{\alpha\beta_1}\left(-g_m V_{out}\right)R \tag{29}$$

However, for CW mode, the circuit analysis is similar to CCW mode, and voltage V_{in2} can be expressed according to equation (10).

5 Simulation Results

The proposed voltage mode Schmitt trigger design illustrated in Fig. 3 is examined with both CMOS and IC AD844 based DVCCTA using PSPICE with 0.18 µm CMOS technology parameter from TSMC. The passive attributes are selected as R=500 Ω and R_m=1 kΩ with 50 Hz sinusoidal input voltage of amplitude ±8 V. Fig. 7 depicts the simulation responses of input and output characteristics for the (current feedback operational amplifier) CFOA based implementation of the proposed design. In addition, the transient response of a proposed Schmitt trigger circuit utilizing CMOS imple-

mentation is illustrated in Fig. 8. The CMOS-based DVCCTA is biased with a supply voltage of $V_{DD} = -V_{SS} = 1.4V$, VB = -0.4V and $I_B = 60$ µA ($g_m = 0.9961$ mS), with R = 500 Ω. Here, gm is calculated to according to equation (2). The aspect ratios of MOS transistor are provided in Table. 2. Besides, the input and output characteristics for the proposed transimpedance mode schmitt trigger with a 50 Hz sinusoidal current input (I_{in}) of ±2 mA amplitude and $R = R_1 = R_2 = 1$ kΩ, $R_m = 10$ kΩ is shown in Fig. 9 and Fig. 10. Furthermore, to check the proposed design's workability at higher frequencies, a 5 MHz sinusoidal voltage waveform with amplitude ±8 V is applied to voltage mode Schmitt trigger design. Fig. 11 depicts that the amplitude levels are not distorted at higher frequencies which further confirms the capability of Schmitt trigger circuits over a wide range of frequency. The CCW Schmitt trigger exhibits a -3 dB bandwidth at approximately 12.86 MHz, while the CW mode shows at around 10.82 MHZ.

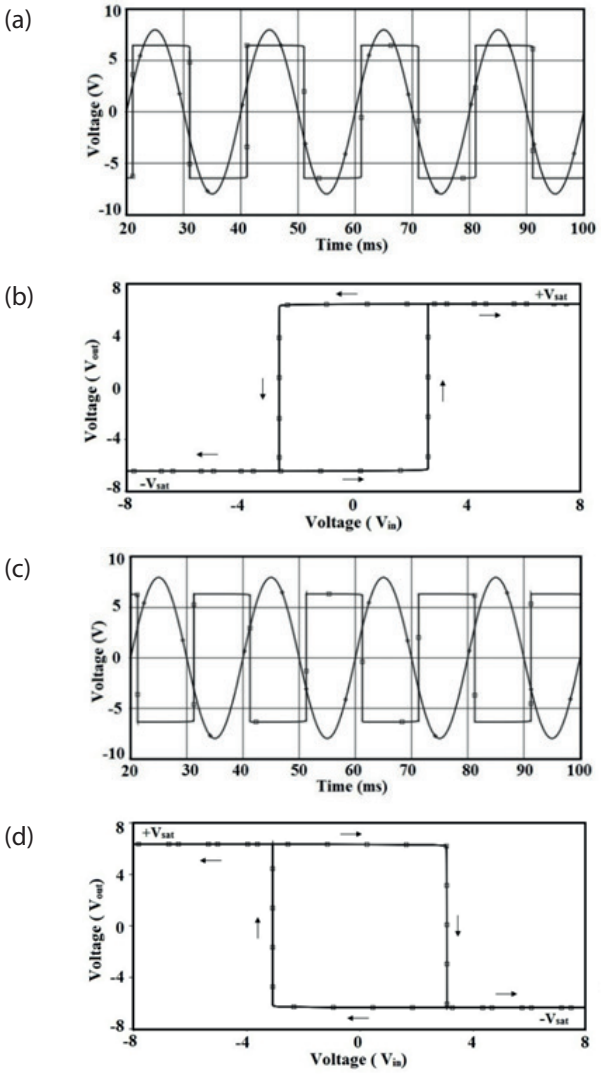

Figure 7: Simulated AD844 based DVCCTA Schmitt trigger responses (a) CCW V_{in1} and V_{out} waveform (b) CCW Hysteresis curve (c) CW V_{in1} and V_{out} waveform (d) CW Hysteresis curve

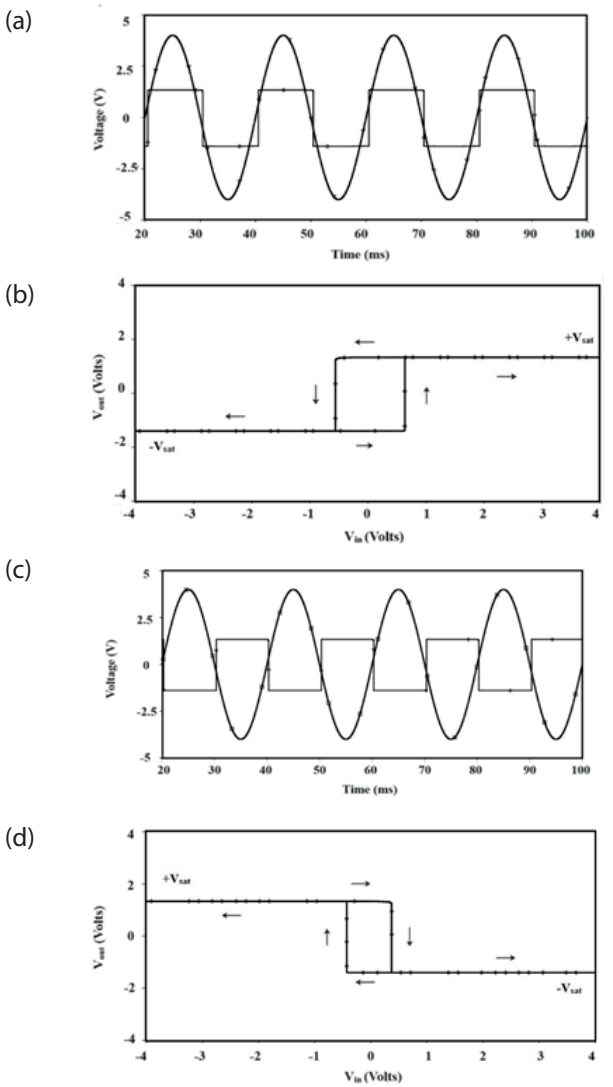

Figure 8: Simulated CMOS based DVCCTA Schmitt trigger responses (a) CCW V_{in1} and V_{out} waveform (b) CCW Hysteresis curve (c) CW V_{in1} and V_{out} waveform (d) CW Hysteresis curve

Table 2: CMOS based DVCCTA transistors dimensions

Transistors	W (in µm)	L (in µm)
M_1 - M_6	4.32	0.36
M_7-M_{10}	1.44	0.36
M_{11}-M_{16}	21.6	0.36
M_{17}-M_{20}	7.2	0.36

In order to evaluate the temperature stability of the proposed Schmitt triggers, the output (V_{out}) is observed at different temperature values specifically (27 °C, 50 °C, 75 °C and 100 °C). As a result, as shown in Fig.12, it is observed that the amplitude and the threshold levels of a square wave are not adversely affected due

(a)

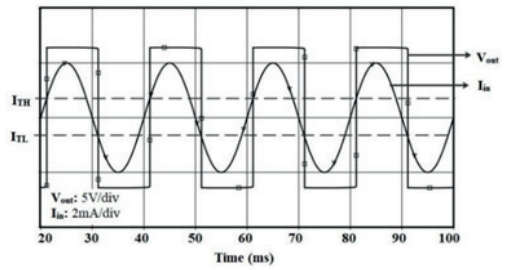

(b)

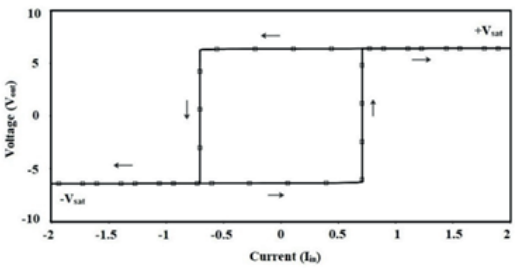

Figure 9: Simulated AD844 based Transimpedance mode CCW operation (a) I_{in1} and V_{out} waveform (b) Hysteresis curve

(a)

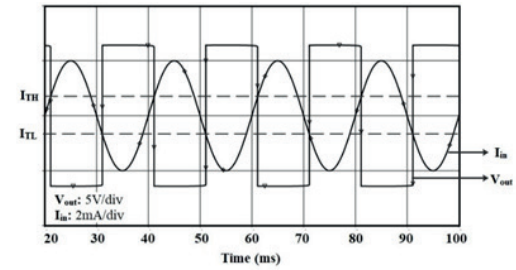

(b)

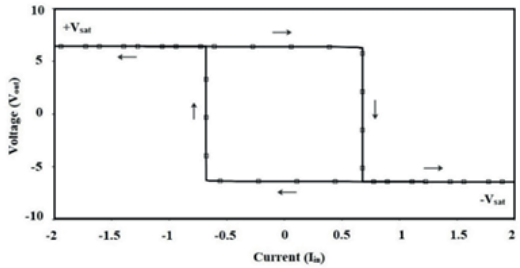

Figure 10: Simulated AD844 based Transimpedance mode CW operation (a) I_{in2} and V_{out} waveform (b) Hysteresis curve

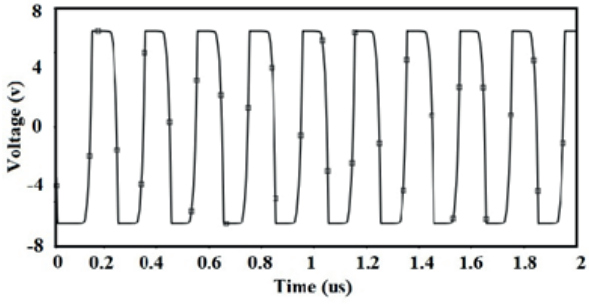

Figure 11: V_{out} at 5 MHz

to temperature variations. To further quantify the extent of deviation in amplitude and threshold levels, it is checked for temperature variations of 0- 100 °C. Notably, the findings from Figs. 13 and 14 reveals that the maximum absolute deviation in output amplitude remains below 0.0625 % (for CW Schmitt trigger) and 0.0381 % (for CCW Schmitt trigger), while for threshold voltages magnitude is less than 0.5 % (for both CW and CCW modes). Moreover, the stability of output amplitude levels through Monte Carlo analysis at temperatures 27, 50, 75 and 100 °C, considering over 200 random points with a 5 % tolerance in resistor values is depicted in Fig. 15 and 16. The measured mean and standard deviation values for output amplitude are as follows: (1.3119, 0.00058), (1.3128, 0.00059), (1.3142, 0.00061), (1.3159, 0.00063) for CCW mode, while for CW mode are taken as (1.2798, 0.0022), (1.2508, 0.0029), (1.2508, 0.003), (1.2515, 0.003), respectively which further demonstrates the circuit's resilience to temperature variations.

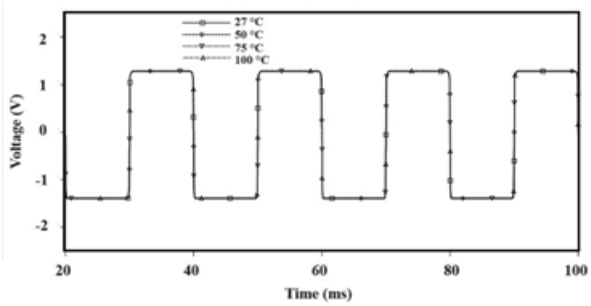

Figure 12: Variation in V_{out} for different temperature values (27 °C, 50 °C, 75 °C, 100 °C)

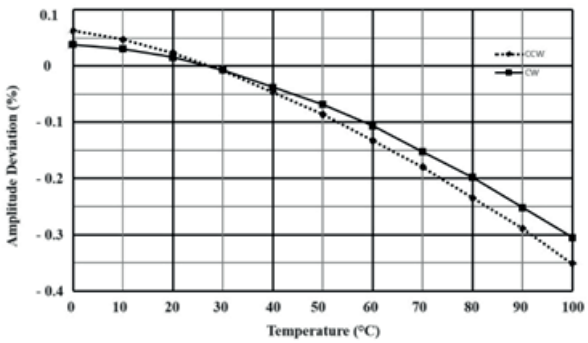

Figure 13: Deviation in output amplitude levels of the proposed voltage mode Schmitt trigger against temperature variations

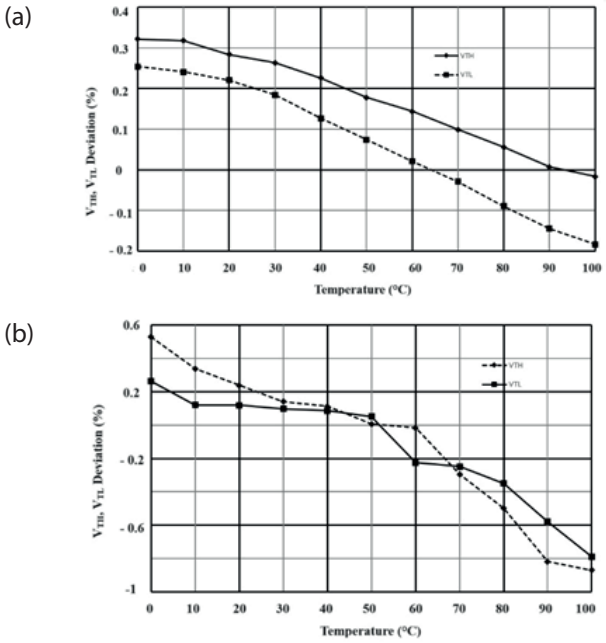

Figure 14: Deviation in Threshold voltage levels against temperature variations (a) CCW Schmitt trigger (b) CW Schmitt trigger

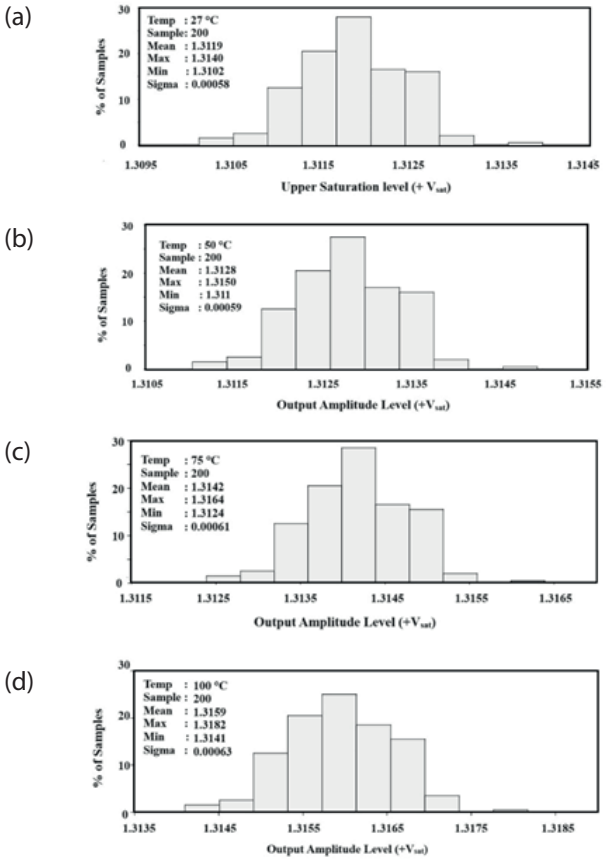

Figure 15: Monte Carlo simulations of output amplitude for CCW mode Schmitt Trigger (a) 27 °C (b) 50 °C (c) 75 °C (d) 100 °C.

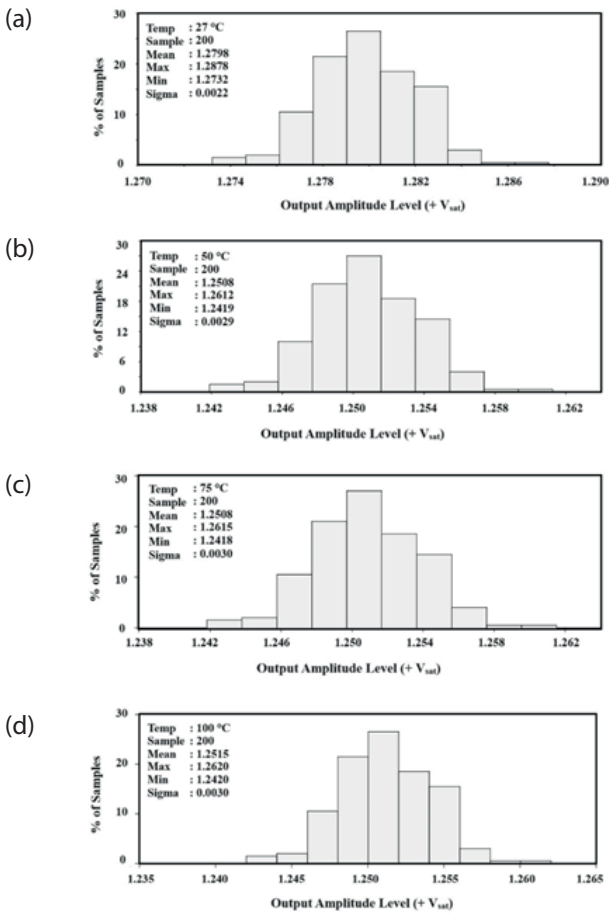

Figure 16: Monte Carlo simulations of output amplitude for CW mode Schmitt Trigger (a) 27 °C (b) 50 °C (c) 75 °C (d) 100 °C.

Fig. 17 depicts the simulated responses of both the CW and CCW structures of the proposed voltage mode circuit for a triangular wave input with a frequency of 50

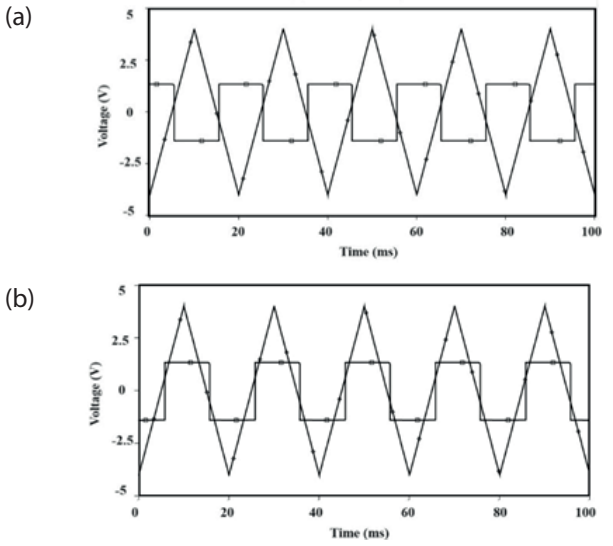

Figure 17: Triangular wave V_{in} and V_{out} waveform (a) CW (b) CCW

Hz and an amplitude of ± 4 V. Subsequently, the output is observed to be a square wave, regardless of the input waveform type. This key characteristic demonstrates the versatility and feasibility of the circuit, as it can effectively process and convert different types of input signals.

From Figs. 18 and 19, it is observed that the threshold levels of the proposed ICAD844 based voltage and transimpedance mode Schmitt trigger circuits can be electronically controlled by adjusting the transconductance parameter (g_m) through the relationship $g_m = \frac{1}{R_m}$, without disturbing the output's amplitude. Figs. 20 and 21 interprets the illustration for theoretical and simulated threshold voltages against R_m variation of dual type voltage mode Schmitt trigger, respectively. It is observed that the simulated threshold values concur well with the theoretical anticipation. Overall, the analysis highlights the controllability of threshold levels through R_m.

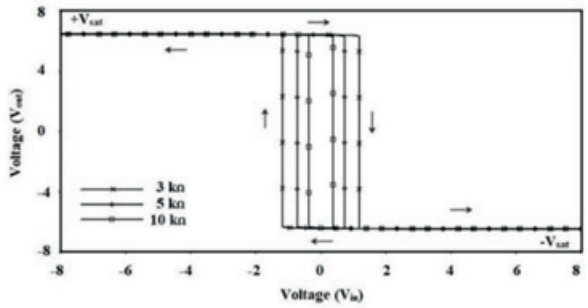

Figure 18: DC transfer characteristic of voltage mode Schmitt trigger for different R_m

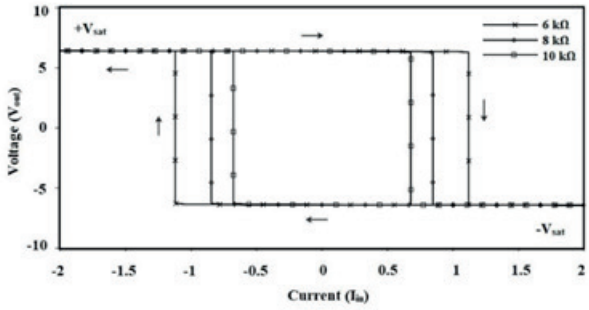

Figure 19: DC transfer characteristic of transimpedance mode Schmitt trigger for different R_m

Fig. 22 exhibits the theoretical simulation results for variation in operating frequency against C_0. The results reveal that the operating frequency can be independently adjusted by C_0, wherein, Equation (20) helps for the theoretical analysis. By maintaining the values of other external components R at 865 Ω and $R_m = R_0 =$ 1 kΩ, the capacitance can be varied from 3.8535 μF to 0.1376 nF. This variation in the capacitor enables a frequency range of 50 Hz to 1.4 MHz, further demonstrating the linearity of the proposed circuit over a broad frequency range. The output transient response of application part of Schmitt trigger as the square/triangular waveform generator at different input frequencies is pictured in Fig. 23 using CMOS based implementation of DVCCTA. The component values are elected as $C_0 =$ 3.8535 μF, R = 865 Ω and $R_m = R_0 =$ 1 kΩ. The summarized key properties of proposed designs is given in Table. 3.

(a)

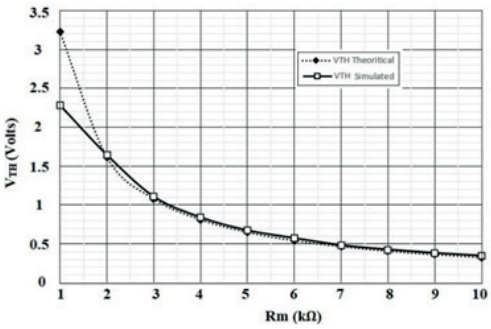

(b)

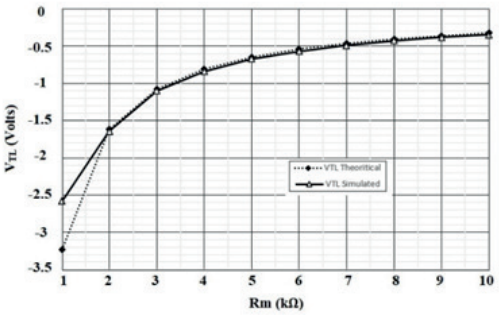

Figure 20: CW Schmitt Trigger threshold voltage levels against R_m (a) V_{TH} (b) V_{TL}

(a)

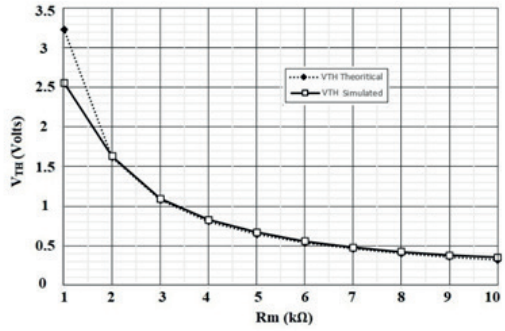

(b)

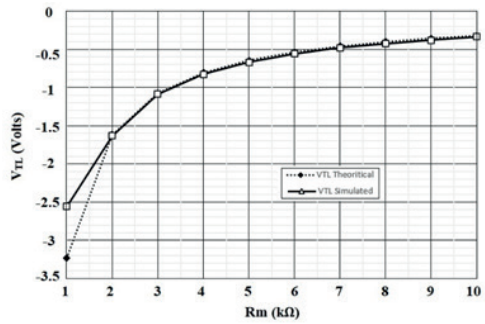

Figure 21: CCW Schmitt Trigger threshold voltage levels against R_m (a) V_{TH} (b) V_{TL}

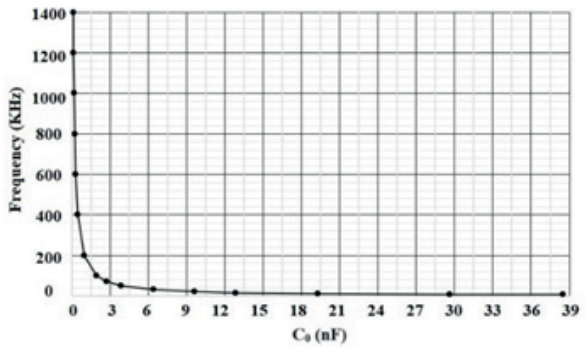

Figure 22: The operating frequency variations with changes in C_o

(a)

(b)

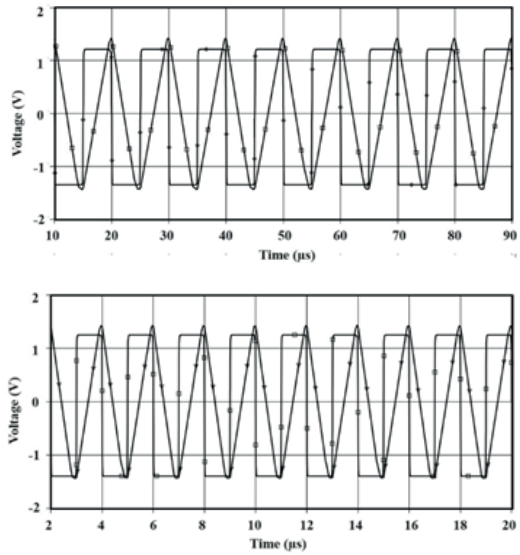

Figure 23: Transient response of Square/triangular waveform generator for input frequency (a) 100 KHz (b) 500 KHz

Finally, the circuit in Fig. 6 is used for the generation of PWM, and its output is depicted in Fig. 24 with the selection of R = 1 kΩ and R_m = 10 kΩ and input voltage V_{in} of 50 Hz sinusoidal with an amplitude of $8V_{pp}$. The carrier waveform V_C of about 500 Hz is set to be a triangular wave. It is obvious that the pulse width of V_{out} is modulated according to the input-modulating sinusoidal signal.

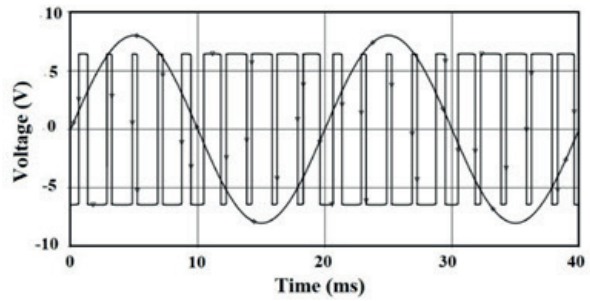

Figure 24: Simulated PWM output

6 Experimental results

The experimental demonstration of the considered design is done by means of IC AD844 implementation of DVCCTA. The supply voltages VDD and VSS for IC AD844 are given as ±15V along with r= 20 kΩ. The proposed voltage mode CW Schmitt trigger at different frequencies gives the transient response as displayed in Fig. 25. Correspondingly, component values for practical verification are selected as R = 1 kΩ and Rm = 10

(a)

(b)

(c)

(d)

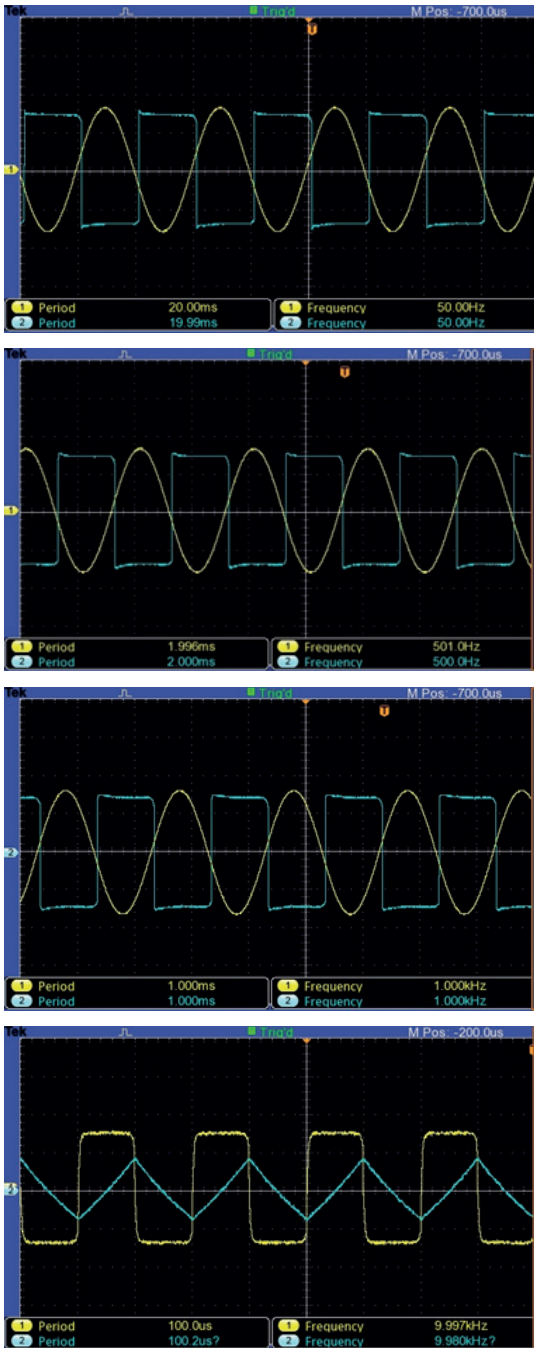

Figure 25: Experimentally observed V_{in} and V_{out} at frequencies (a) 50 Hz (b) 500 Hz (c) 1 kHz (d) 10 kHz

Table 3: Summary of key attributes of proposed Schmitt trigger circuits.

Parameters	CW Schmitt Trigger		CCW Schmitt Trigger	
No. of AAB (DVCCTA) used	1			
No. of passive elements used	1 (grounded)			
Maximum operational frequency	10.82 MHz		12.86 MHz	
Output amplitude levels deviation for temperature variations (0-100 °C)	Less than 0.0381 %		Less than 0.0625 %	
Threshold levels deviation for temperature variations (0-100 °C)	Less than 0.5282 %		Less than 0.3216 %	
Temperatures	Mean	Standard deviation	Mean	Standard deviation
27 °C	1.2798	0.0022	1.3119	0.00058
50 °C	1.2508	0.0029	1.3128	0.00059
75 °C	1.2508	0.003	1.3142	0.00061
100 °C	1.2515	0.003	1.3159	0.00063
Power supply	1.4 V			
Power Consumption	3.51 mW			
Application (Square/triangular wave generator) – Frequency range for capacitance variation (3.8535 µF to 0.1376 nF)	50 Hz – 1.4 MHz			

kΩ with a sinusoidal input voltage of amplitude $V_{in} = \pm 8$ V. Accordingly, Fig. 26 delivers the output waveform for square/triangular wave generator with the selection of $R_m = R_O = R = 1$ kΩ and the variation of C_0 as 3.33 μF, 0.33 μF, 0.11 μF, 0.01 μF *for* different frequencies of 50 Hz, 500 Hz, 1 kHz, 10 kHz respectively.

Moreover, Fig. 27 demonstrates the experimental output for PWM signal in transient domain with an input voltage V_{in} of 50 Hz, $8V_{pp}$ sinusoidal and V_C works as the carrier signal which is preferred to be a triangular waveform. The component values are selected as R = 1 KΩ and R_m = 10 KΩ. It is observed that the width of the modulated output signal is controlled by controlling input voltage V_{in} with respect to carrier signal voltage.

Additionally, the MOS based schematic layout of the proposed Schmitt trigger for Fig. 2 (b) has been de-

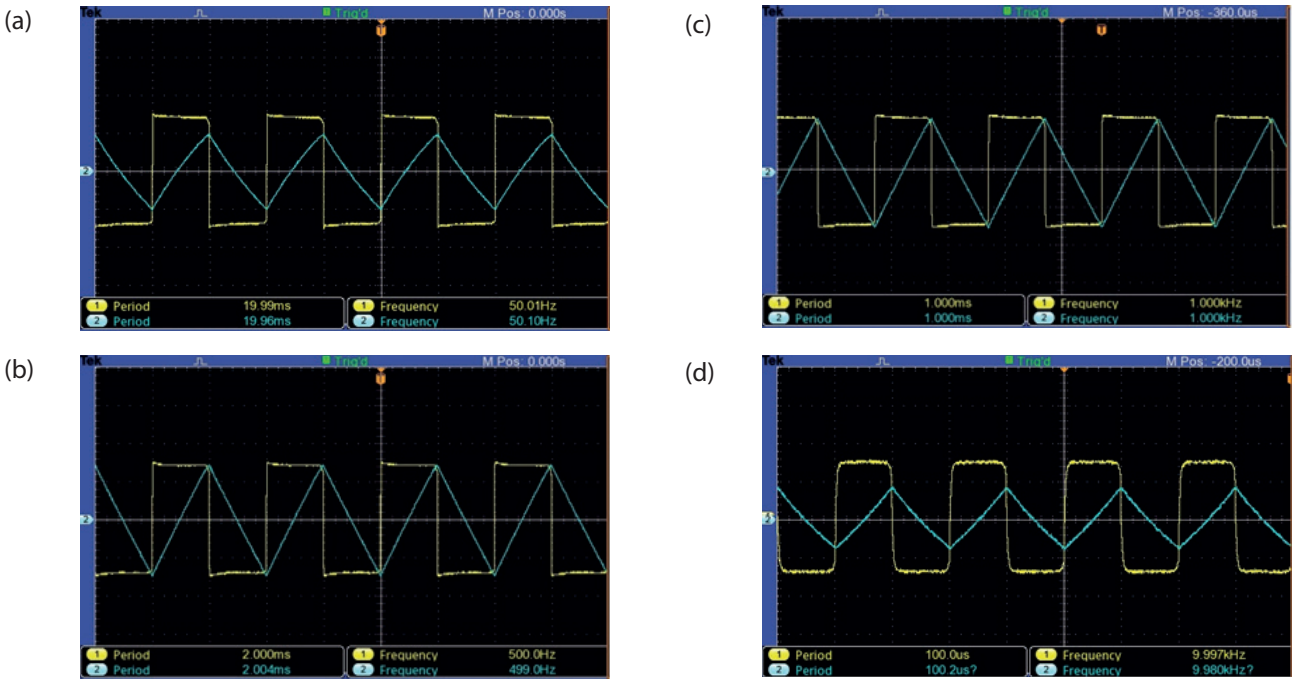

Figure 26: Experimentally observed V_{out1} and V_{out2} at frequencies (a) 50 Hz (b) 500 Hz (c) 1 kHz (d) 10 kHz

signed in virtuoso Analog Design Environment of the cadence software using 180 nm gpdk CMOS process parameters, is depicted in Fig. 28, showcasing its physical design. Furthermore, the accuracy of the layout has been assessed by conducting error checking and comparing nets between schematic and layout using specific tools, namely Design Rule Checking (DRC) and Layout Versus Schematic (LVS) verification. The pre-layout and post-layout simulations of the proposed Schmitt trigger are carried out which are given in Fig. 29.

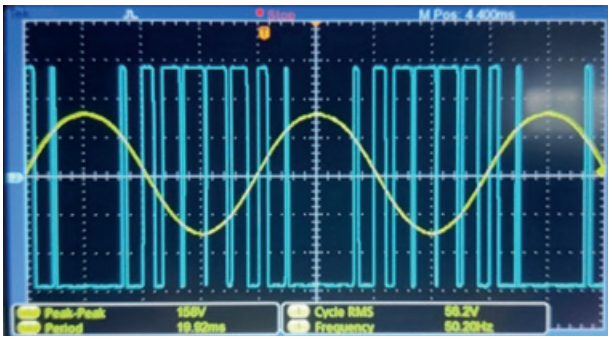

Figure 27: Modulating input V_{in} and PWM output waveform

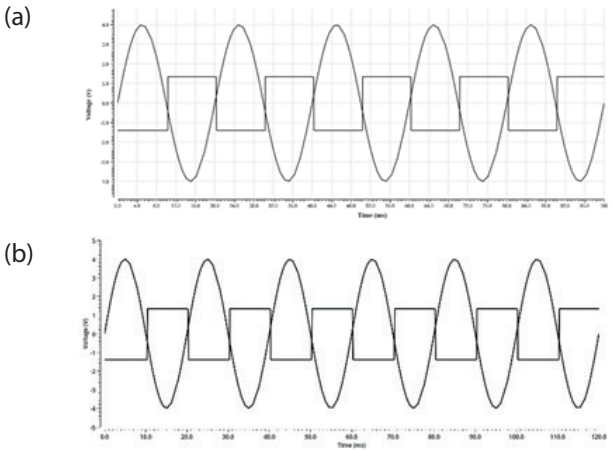

Figure 29: Input and output waveforms of proposed Schmitt trigger (a) Pre-layout simulation (b) Post-layout simulation

7 Comparison

Table. 1 provides a comprehensive comparison between the proposed topologies and the existing models found in the literature. The significance of

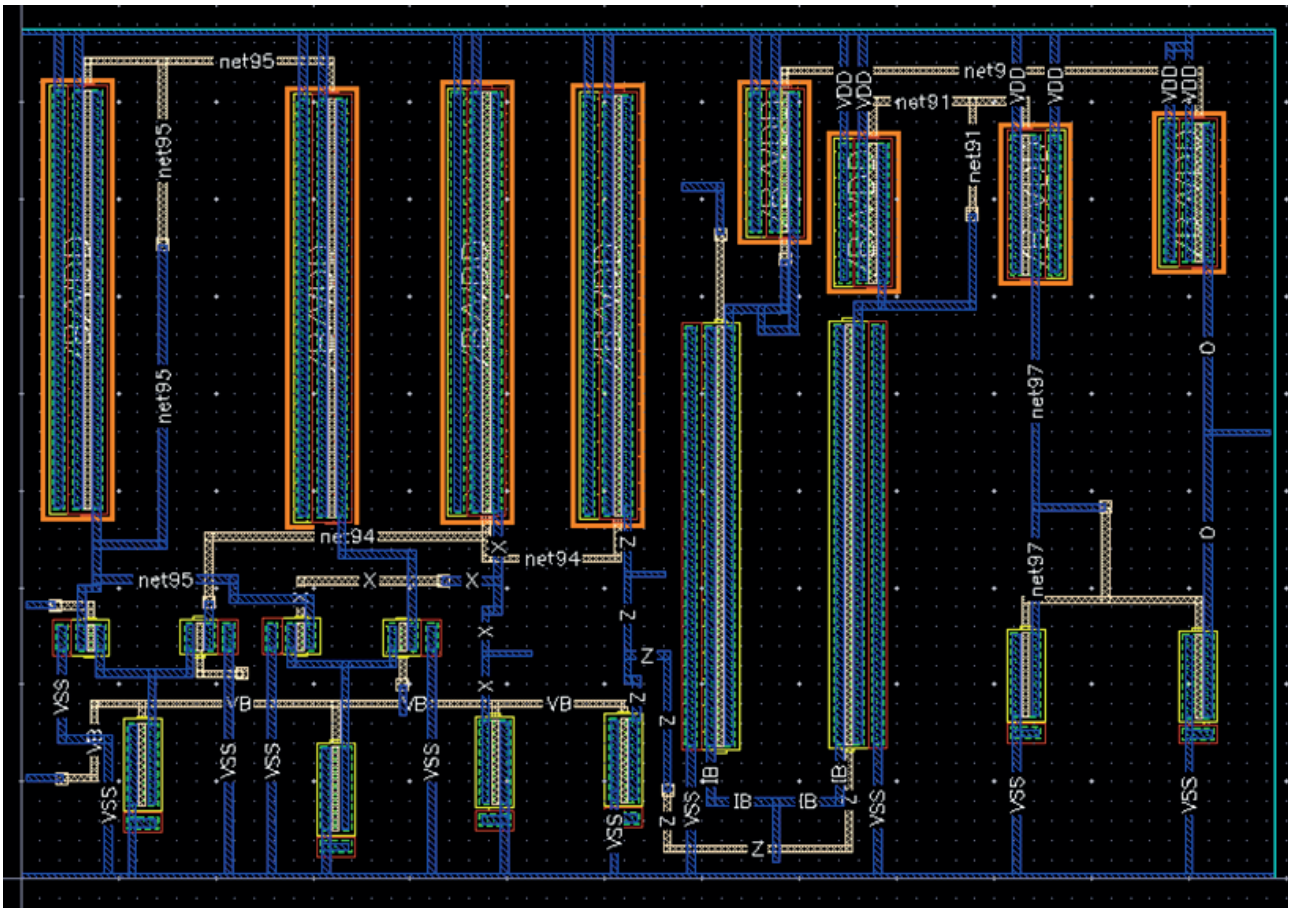

Figure 28: Schematic Layout of DVCCTA for proposed design

the proposed designs is more precisely well summarized as:

- Use of a greater number of active elements [23, 25, 28, 43].
- Use of many passive attributes [23-25, 27-28, 31-33, 35, 38-43].
- Absence of dual-type hysteresis mode of operation [23-25, 27, 28, 30-33, 37-40, 42].
- Absence of dual type hysteresis mode of operation within the same topology [23-25, 27, 28, 30-33, 35, 37-40, 42].
- Absence of Independent control of threshold levels [23-25, 27, 29, 32-33, 35, 38-40, 42]
- Absence of Independent control of oscillation frequency [23-24, 29- 30, 32, 34-35, 37-38,43]
- Use of floating passive elements, which is difficult for IC fabrication [23-25, 27, 29, 32, 33, 35, 39-40, 42-43].

Based on the aforementioned observations, it is evident that the proposed Schmitt trigger circuits offer several notable advantages.

- Use of single AAB for realization of proposed circuits.
- Use of less number of grounded passive elements which makes it suitable for IC integration.
- Provides dual-mode Schmitt trigger circuits with single DVCCTA and grounded resistors.
- Provides both modes (CW and CCW) within the same topology.
- Extended for the application of square/triangular waveform generator and pulse width modulator.
- Provides good operational frequency.
- Independent control of Hysteresis.
- Independent control of the frequency of oscillation through a grounded capacitor.
- Insensitive to temperature.

8 Conclusion

Novel dual-mode Schmitt trigger employing a single DVCCTA and its application to square/triangular wave generator constructed using an additional CFOA, a grounded capacitor, and a grounded resistor which comprises an integrator and pulse width modulator (PWM) within the same topology is presented. The proposed design avails of two modes specifically voltage and transimpedance modes where the CW and CCW type of operation is acquired within the same topology on the basis of the selection of input. It uses only grounded passive elements and also a single CMOS-based DVCCTA, which is suitable for IC integration. Additionally, independent control of threshold levels is available. Tunability of grounded components is the prominent feature of the design where the operating frequency can be made adjustable using a grounded capacitor and reduces the level of parasitics which sets the proposed design insensitive to noise. The highest absolute deviation of output amplitude and threshold voltage is less than 0.062 % and 0.528 %, respectively, over temperature variations ranging from 0- 100^0 C. The design brings dual-mode dual-type hysteresis operation, an excellent operational frequency range, and also insensitivity to temperature variations. Monte Carlo simulations, non-ideal analysis, and experimental results as well as the schematic layout with post-layout simulation results are depicted to justify the considered structure. The unique characteristics of the proposed designs make them applicable for bio-medical and other signal processing applications and can be extended for designing relaxation oscillators, versatile modulators, monostable multivibrators, etc.

9 Acknowledgments

This research is supported by Chips2startup (C2S) project sponsored by MEITY, Govt. of India and sanctioned to NIT Andhra Pradesh cluster.

10 Conflict of Interest

The authors declare that they have no conflict of interest.

Data Availability Statement: Data sharing not applicable to this article as no datasets were generated or analysed during the current study.

11 References

1. A. Sedra, K. C. Smith, "Microelectronic Circuits : 4th edition," oxford: Oxford University Press.ISBN 9780195116632.
2. S. K. Kar and S. Sen, "Tunable square-wave generator for integrated sensor applications," *IEEE Trans. Instrum. Meas.*, vol. 60, no. 10, pp. 3369–3375, 2011, https://doi.org/10.1109/TIM.2011.2128490.
3. P. Tuwanut, J. Koseeyaporn, and P. Wardkein, "A novel versatile modulator circuit," *AEU - Int. J. Electron. Commun.*, vol. 63, no. 5, pp. 387–397, 2009, https://doi.org/10.1016/j.aeue.2008.02.010.
4. T. Onomi, "Experimental Demonstration and Performance Estimation of a new Relaxation Oscillator Using a Superconducting Schmitt Trigger Inverter," *Phys. Procedia*, vol. 81, pp. 141–144, 2016, https://doi.org/10.1016/j.phpro.2016.04.030.

5. D. Kumar and R. Khatri, "Function Generator using Current Conveyor (CCII)," *Int. J. Comput. Appl.*, vol. 147, no. 7, pp. 1–4, 2016, https://doi.org/10.5120/ijca2016911163.
6. H. C. Chien and Y. K. Lo, "Design and implementation of monostable multivibrators employing differential voltage current conveyors," *Microelectronics J.*, vol. 42, no. 10, pp. 1107–1115, 2011, https://doi.org/10.1016/j.mejo.2011.07.005.
7. R. K. Ranjan, K. Mazumdar, R. Pal, and S. Chandra, "Generation of square and triangular wave with independently controllable frequency and amplitude using OTAs only and its application in PWM," *Analog Integr. Circuits Signal Process.*, vol. 92, no. 1, pp. 15–27, 2017, https://doi.org/10.1007/s10470-017-0971-x.
8. R. L. Newsom, W. C. Dillard, and R. M. Nelms, "Digital power-factor correction for a capacitor-charging power supply," *IEEE Trans. Ind. Electron.*, vol. 49, no. 5, pp. 1146–1153, 2002, https://doi.org/10.1109/TIE.2002.803240.
9. C. Toumazou, F. J. Lidgey, D. G. Haigh, "Analogue IC Design: the Current-Mode Approach," London: Peter Peregrinus Ltd. ISBN 0863412971.
10. D. Biolek, R. Senani, V. Biolkova, and Z. Kolka, "Active elements for analog signal processing: Classification, review, and new proposals," *Radioengineering*, vol. 17, no. 4, pp. 15–32, 2008.
11. A. Sedra, K. C. Smith, "A second generation current conveyor and its applications," *IEEE Trans. Circuit Theory*, vol. 17, no. 1, pp. 132–134, 1970.
12. A. Fabre, "Third generation current conveyor: A new helpful active element," *Electronic Letters*, vol. 31, no. 5, pp. 338–339, 1995.
13. R. V Golhar, M. A. Gaikwad, and V. G. Nasre, "Design and Analysis of High Performance Operational Transconductance Amplifier," *International Journal of Scientific and Research Publivations,* vol. 2, no. 8, pp. 1–5, 2012.
14. A. K. Singh, R. Senani, and A. Gupta, "OTRA, its implementations and applications: a state-of-the-art review," vol. 97, no. 2. Springer US, 2018.
15. H. O. Elwan, A. M. Soliman, "Novel CMOS differntial voltage current conveyor and its applications," *IEEE Proceedings: Circuits, Devices and Systems*, vol. 144, no. 3, pp. 195-200, 1997.
16. A. Zeki and A. Toker, "The dual-X current conveyor (DXCCII): A new active device for tunable continuous-time filters," *Int. J. Electron.*, vol. 89, no. 12, pp. 913–923, 2002, https://doi.org/10.1080/0020721031000120461.
17. A. Kumar and B. Chaturvedi, "Novel CMOS Dual-X Current Conveyor Transconductance Amplifier Realization with Current-Mode Multifunction Filter and Quadrature Oscillator," *Circuits, Syst. Signal Process.*, vol. 37, no. 6, pp. 2250–2277, 2018, https://doi.org/10.1007/s00034-017-0680-9.
18. N. Pandey and R. Pandey, "a First Order All Pass Filter and Its Application in a Quadrature Oscillator," vol. 12, pp. 772–777, 2012.
19. S. K. Paul and N. Pandey, "VM and CM universal filters based on single DVCCTA," *Act. Passiv. Electron. Components*, vol. 2011, 2011, https://doi.org/10.1155/2011/929507.
20. H. C. Chien and C. Y. Chen, "CMOS realization of single-resistance-controlled and variable frequency dual-mode sinusoidal oscillators employing a single DVCCTA with all-grounded passive components," *Microelectronics J.*, vol. 45, no. 2, pp. 226–238, 2014, https://doi.org/10.1016/j.mejo.2013.11.007.
21. N. Pandey and R. Pandey, "Approach for third order quadrature oscillator realisation," *IET Circuits, Devices Syst.*, vol. 9, no. 3, pp. 161–171, 2015, https://doi.org/10.1049/iet-cds.2014.0170.
22. W. Tangsrirat, "Floating simulator with a single DVCCTA," *Indian J. Eng. Mater. Sci.*, vol. 20, no. 2, pp. 79–86, 2013.
23. A. Srinivasulu, "A novel current conveyor based Schmitt trigger and its application as a relaxation Oscillator," *Int. J. Circuit Theory Appl.*, vol. 39, pp. 679–686, 2011.
24. S. Del Re, A. De Marcellis, G. Ferri, and V. Stornelli, "Low voltage integrated astable multivibrator based on a single CCII," *Proc. 2007 Ph.D Res. Microelectron. Electron. Conf. PRIME 2007*, no. 2, pp. 177–180, 2007, https://doi.org/10.1109/RME.2007.4401841.
25. A. De Marcellis, C. Di Carlo, G. Ferri, and V. Stornelli, "A CCII-based wide frequency range suare waveform generator," *Int. J. Circuit Theory Appl.*, vol. 41, no. 1, 2011.
26. G. Diutaldo, G. Palumbo, and S. Pennisi, "A schmitt trigger by means of a ccii+," *Int. J. Circuit Theory Appl.*, vol. 23, no. 2, pp. 161–165, 1995, https://doi.org/10.1002/cta.4490230207.
27. A. De Marcellis, G. Ferri,, P. Mantenuto, "A CCII-based non inverting Schmitt Trigger and its application as astable multivibrator for capacitive sensor interfacing," *Int. J. Circuit Theory Appl.*, vol. 45, pp. 1060–1076, 2016.
28. W. S. Chung, H. Kim, H. W. Cha, and H. J. Kim, "Triangular/square-wave generator with independently controllable frequency and amplitude," *IEEE Trans. Instrum. Meas.*, vol. 54, no. 1, pp. 105–109, 2005, https://doi.org/10.1109/TIM.2004.840238.
29. Y. K. Lo, H. C. Chein, H. J. Chiu, "Current input OTRA Schmitt trigger with dual hysteresis modes," *Int. J. Circuit Theory Appl.*, vl. 38, pp. 739–746, 2010.
30. A. Kumar and B. Chaturvedi, "Novel electronically controlled current-mode Schmitt trigger based on single active element," *AEU - Int. J. Electron.*

Commun., vol. 82, pp. 160–166, 2017, https://doi.org/10.1016/j.aeue.2017.08.007.
31. S. Minaei and E. Yuce, "A simple Schmitt trigger circuit with grounded passive elements and its application to square/triangular wave generator," *Circuits, Syst. Signal Process.*, vol. 31, no. 3, pp. 877–888, 2012, https://doi.org/10.1007/s00034-011-9373-y.
32. R. Das, K. Banerjee, A. Chakraborty, and L. Mondal, "Differential Difference Current Conveyor (DDCC) Based Schmitt Trigger Circuit & Its Application," *International Journal on Recent and Innovation Trends in computing and Communication*, Vol. 4, no. 8, pp. 69–72, 2016.
33. K. Nagalakshmi, A. Srinivasulu, C. Ravariu, V. Vijay, and V. V. S. V. Krishna, "A Novel Simple Schmitt Trigger Circuit using CDTA and its application as a Square-Triangular Waveform Generator," *J. Mod. Technol. Eng.*, vol. 3, no. 3, pp. 205–216, 2018.
34. A. Kumar and B. Chaturvedi, "Fully electronically controllable Schmitt trigger circuit with dual hysteresis," *Electron. Lett.*, vol. 53, no. 7, pp. 459–461, 2017, https://doi.org/10.1049/el.2016.4770.
35. R. Pal, R. Pandey, N. Pandey, and R. C. Tiwari, "Single CDBA Based Voltage Mode Bistable Multivibrator and Its Applications," *Circuits Syst.*, vol. 06, no. 11, pp. 237–251, 2015, https://doi.org/10.4236/cs.2015.611024.
36. P. Silapan and M. Siripruchyanun, "Fully and electronically controllable current-mode Schmitt triggers employing only single MO-CCCDTA and their applications," *Analog Integr. Circuits Signal Process.*, vol. 68, no. 1, pp. 111–128, 2011, https://doi.org/10.1007/s10470-010-9593-2.
37. M. Siripruchyanun, P. Satthaphol, and K. Payakkakul, "A Simple Fully Controllable Schmitt Trigger with Electronic Method Using VDTA," *Appl. Mech. Mater.*, vol. 781, no. 1, pp. 180–183, 2015, https://doi.org/10.4028/www.scientific.net/amm.781.180.
38. U. Mohammad, M. Y. Yasin, R. Yousuf, and I. Anwar, "A novel square wave generator based on the translinear circuit scheme of second generation current controlled current conveyor-CCCII," *SN Appl. Sci.*, vol. 1, no. 6, 2019, https://doi.org/10.1007/s42452-019-0608-z.
39. V. Vijay and A. Srinivasulu, "A novel squarewave generator using second-generation differential current conveyor," *Arab. J. Sci. Eng.*, vol. 42, no. 12, pp. 4983–4990, 2017, https://doi.org/10.1007/s13369-017-2539-6.
40. V. Vijay and A. Srinivasulu, "A low power waveform generator using DCCII with grounded capacitor," *Int. J. Public Sect. Perform. Manag.*, vol. 5, no. 2, pp. 134–145, 2019, https://doi.org/10.1504/IJPSPM.2019.099084.
41. P. Moonmuang, S. Unhavanich and W. Tangsrirat, "Simple current-controlled VDTA-R Schmitt trigger circuit," *In 2019 5th International Conference on Engineering, Applied Sciences and Technology (ICEAST)*, pp. 1-4, 2019, https://doi.org/10.1109/ICEAST.2019.8802589.
42. A. Kumar and B. Chaturvedi, "Experimental realization of square/triangular wave generator using commercially available ICs," *J. Circuits, Syst. Comput.*, vol. 29, no. 14, 2020, https://doi.org/10.1142/S0218126620502242.
43. A. Anand and R. Pandey, "A Novel Dual Output Schmitt Trigger Using Second Generation Voltage Controlled Conveyor," *2022 2nd International Conference on Intelligent Technologies (CONIT)*, Hubli, India, pp. 1-5, 2022, https://doi.org/10.1109/CONIT55038.2022.9848259.
44. A. Jantakun, N. Pisutthipong, and M. Siripruchyanun, "A synthesis of temperature insensitive/electronically controllable floating simulators based on DV-CCTAs," *2009 6th Int. Conf. Electr. Eng. Comput. Telecommun. Inf. Technol. ECTI-CON 2009*, vol. 1, no. May 2014, pp. 560–563, 2009, https://doi.org/10.1109/ECTICON.2009.5137069.
45. M. S. Roden, "Analog and Digital Communication Systems: 4th edition," Prentice - Hall, Englewood Cliffs, NJ, USA, pp. 176-183, 1996.
46. D. Maksimovic and S. Cuk, "A unified analysis of PWM converters in discontinuous modes," *IEEE Trans. Power Electron.*, vol. 6, no. 3, pp. 476–490, 1991, https://doi.org/10.1109/63.85890.
47. A. Djemouai, M. Sawan, and M. Slamani, "New CMOS integrated pulse width modulator for voltage conversion applications," *Proc. IEEE Int. Conf. Electron. Circuits, Syst.*, vol. 1, no. 2, pp. 116–119, 2000, https://doi.org/10.1109/ICECS.2000.911498.
48. W. Mathis, "Nonlinear systems and communications systems," *5th Int. Conf. Telecommun. Mod. Satell. Cable Broadcast. Serv. TELSIKS 2001 - Proc. Pap.*, vol. 1, no. September, pp. 293–296, 2001, https://doi.org/10.1109/TELSKS.2001.954894.
49. S. V. Singh and C. Shankar, "A new Trans-Impedance Mode biquad filter employing single DVCCTA", Journal of Electrical Systems, Vol. 15, pp. 249-263, 2019.

Arrived: 07. 02. 2024
Accepted: 18. 05. 2024